UC Berkeley
Working Papers

Title
Vehicle Longitudinal Control Test

Permalink
https://escholarship.org/uc/item/42d7r9vg

Author
Choi, Sei-bum

Publication Date
1994

eScholarship.org Powered by the California Digital Library
University of California

This paper has been mechanically scanned. Some errors may have been inadvertently introduced.

CALIFORNIA PATH PROGRAM
INSTITUTE OF TRANSPORTATION STUDIES
UNIVERSITY OF CALIFORNIA, BERKELEY

Vehicle Longitudinal Control Test

Sei-Bum Choi

California PATH Working Paper

UCB-ITS-PWP-94-15

This work was performed as part of the California PATH Program of the University of California, in cooperation with the State of California Business, Transportation, and Housing Agency, Department of Transportation; and the United States Department Transportation, Federal Highway Administration.

The contents of this report reflect the views of the authors who are responsible for the facts and the accuracy of the data presented herein. The contents do not necessarily reflect the official views or policies of the State of California. This report does not constitute a standard, specification, or regulation.

October 1994

ISSN 1055-1417

Vehicle Longitudinal Control Test

Sei-Bum Choi
California PATH
Institute of Transportation Studies
University of California at Berkeley

Abstract

This report evaluates several engine torque control laws for longitudinal vehicle control. The control laws are implemented on Lincoln TownCars and tested on the low speed test track at Richmond Field Station. The test results and analysis show that engine manifold air-dynamics can not be neglected especially at low engine speed. An ultrasonic distance sensor is evaluated under several road conditions. Two vehicle tracking control is tested using the ultrasonic sensor and radio transceivers.

Key Words

Advanced Vehicle Control Systems, Longitudinal Control, Testing, Vehicle Following

1 Introduction

The California Partners for Advanced Transit and Highway (PATH) are developing automated vehicle control systems (AVCS) required for ITS, and a number of engine control laws for longitudinal control have been developed and compared by simulation [2][6].

However, in many cases, simulation results can be quite different from experimental results due to the effect of unknown modeling errors. In this report, several control laws are implemented on the test vehicles using a Quick-C compiler and XIGNAL, a real-time scheduler. The relative performance of the control laws are compared by single vehicle speed tracking. The Polaroid ultrasonic ranging system is evaluated under several driving conditions. Two vehicle tracking control is performed using the ultrasonic sensor and radio transceivers.

2 Vehicle Model for Longitudinal Control

This section describes a vehicle model for longitudinal speed control. The model is based on Cho and Hedrick's continuous engine model[1]. The sub-models considered are engine, intake manifold and torque converter.

2.1 Engine

The continuous engine model is described by:

$$\dot{\omega}_e = \frac{1}{I_e}\left[T_{net}(\omega_e, m_a) - T_L\right] \tag{1}$$

where T_{net} is the net combustion torque (indicated torque $-$ friction torque), T_L the external torque on the engine, I, the equivalent rotational inertia of the vehicle on the engine, ω_e the engine speed and m_a the mass of air in the intake manifold. If each cylinder event is neglected and a constant air-to-fuel ratio assumed, T_{net} is a function of only ω_e and m_a.

2.2 Intake Manifold

The assumptions in the modeling of the intake manifold are:

- the air in the intake manifold obeys the ideal gas law
- all properties (pressure and temperature) are uniform throughout the volume of the manifold

- the temperature of the air in the manifold is constant or changing very slowly
- the presence of fuel has no effect on the air flow
- the amount of E.G.R. (exhaust gas recirculation) is negligibly small.

Neglecting the effects of individual intake strokes and resulting pulsation of the air, the continuity equation of the manifold volume is:

$$\dot{m}_a = \dot{m}_{ai}(\alpha, P_m/P_{atm}) - \dot{m}_{ao}(\omega_e, m_a) \tag{2}$$

$$P_m V_m = m_a R T_m \tag{3}$$

where $\dot{m}_{ai}$ means the air flow rate through the throttle body, $\dot{m}_{ao}$ the air flow rate into the cylinder, α the throttle angle, P_m the manifold air pressure, P_{atm} the atmospheric air pressure, V_m the manifold volume, R the ideal gas constant and T_m the manifold air temperature.

2.3 Torque Converter

The torque converter consists of a pump attached to the engine and a turbine attached to the driving axle through a transmission. Neglecting the inertia of the transmission oil in the converter, it can be assumed to be a static element. On each side, the torque is related to the speed by:

$$T_t = \left(\frac{\omega_t}{C_{tr}}\right)^2 \tag{4}$$

$$T_p = \left(\frac{\omega_p}{C_{pr}}\right)^2 \tag{5}$$

where (T_t, ω_t, C_{tr}) and (T_p, ω_p, C_{pr}) are the torques, the speeds and the capacity factors of the turbine and the pump. Since capacity factors are functions of the speed ratio($\stackrel{\mathbf{A}}{=} \omega_t/\omega_p$), T_t, ω_t, T_p and ω_p are coupled to each other, and the change of one affects the other three.

3 Control Laws

All the control laws in this section are derived under a no-slip condition of the driving wheels, i.e.:

$$V = R h w, \tag{6}$$

where V is the vehicle speed, R the gear ratio from the engine to the wheels and h the tire radius of the driving wheels. If the platoon spacing error $S_1(\triangleq P - P_{des},\ \dot{P} = V)$satisfies:

$$\ddot{S}_1 + 2\,\zeta\,\omega_n\,\dot{S}_1 + \omega_n^2\,S_1 = 0 \tag{7}$$

,where ζ and ω_n are design variables to be chosen depending upon the requirement of the control, then the error S_1 will go to zero asymptotically. Substituting equations (1)and (6) into equation (7), the desired engine torque for equation *(7)* to be satisfied is:

$$T_{net_des} = I_e\left[\dot{\omega}_{e_des} - 2\,\zeta\,\omega_n\,(\omega_e - \omega_{e_des}) - \frac{\omega_n^2\,S_1}{R\,h}\right] + T_L \tag{8}$$

If the manifold air dynamics are neglected, $\dot{m}_{ai} = \dot{m}_{ao}$, and T_{net} becomes a function of ω_e and a, and the desired throttle angle α_{des} can be obtained as:

$$\alpha_{des} = \alpha_{des}(T_{net_des},\,\omega_e) \tag{9}$$

If the manifold air dynamics are not neglected, T_{net} is a function of ω_e and m_a. Therefore, the desired air mass m_{a_des} for S_1 to satisfy equation *(7)* is obtained as:

$$m_{a_des} = m_{a_des}(T_{net_des},\,\omega_e) \tag{10}$$

Since m_{a_des} is not an explicit function of the control α, define:

$$S_2 \triangleq m_a - m_{a_des} \tag{11}$$

and, let S_2 satisfy:

$$\dot{S}_2 = -\lambda_2\,S_2\ ,\quad \lambda_2 > 0 \tag{12}$$

then, substituting equation (2) into equation (12):

$$\dot{m}_{ai_des}(\alpha_{des},\,P_m/P_{atm}) = \dot{m}_{ao} + \dot{m}_{a_des} - \lambda_2\,(m_a - m_{a_des}) \tag{13}$$

or

$$\alpha_{des} = \alpha_{des}(\dot{m}_{ai_des},\,P_m/P_{atm}) \tag{14}$$

Here, $\dot{m}_{ao}$ is a function of ω_e and m_a, and using m_{a_des}(or P_{m_des}) instead of m_a(or P_m) makes the closed loop system more stable[2]. Due to the same reason, P_{m_des} is used instead of P_m in α_{des}.

In the lower(first and second) gear states, the engine is not connected to the driving wheels mechanically, and there exists torque converter slip. Especially very low wheel speeds, the slip is not negligibly small and the torque converter should be considered in the control loop, since the turbine torque is much bigger than the pump torque and the resulting control input is too much. However, at $10\,m/sec$ and above, the slip is negligible.

4 Single Vehicle Test

This section describes the implementation of the control laws derived in section **3** on a test vehicle to follow the desired speed trajectories of an artificial lead vehicle. Since there exists no error in measuring the distance and the rate of change between the vehicles, the tracking performance can be much better than that in true vehicle following using real sensors.

All the tests in this section were performed in first gear and there was no brake force on the wheels except that from the engine brake torque.

4.1 Simple Model

Figure **4.1** shows the test result of the control law given in equations **(8)** and (9) without the torque converter effect being compensated. Even though critical damping ((= **1)** is intended in the closed-loop, there exists a mode with zero or quite small damping, and the torque converter compensation is of no help in suppressing this mode (see figure **4.2).** Figure **4.3** shows that the zero damping mode disappears at higher vehicle speeds or equivalently higher engine speeds. Due to this mode, the tracking performance deteriorates quickly as the frequency of the desired tracking speed profile is increased from **0.1** Hz to **0.2** Hz(see figure **4.4).**

4.2 Full Model

Figure **4.5** shows the test result of the control law given in equations (8), (10), **(13)** and **(14)** without the torque converter compensation. The transient error disappears quickly and the zero damping mode does not appear even after some maneuvering. At the very low vehicle speed, the turbine torque is much bigger than the pump torque and the control law, which neglects this effect, causes overshoot (see figure **4.5;** 0 - **3** sec., **12 - 14** sec.). The throttle, and therefore the vehicle acceleration, can be smoothed without causing any delay **by** compensation of the torque converter effect (see figure **4.6).** This control law based on a full engine model does not exhibit bad effects such **as** chattering at the higher vehicle (or engine) speed (see figure **4.7),** and tracking the higher frequency speed profile is possible since the zero damping mode is suppressed (see figure **4.8).**

4.3 Evaluation

The cause of the zero damping mode, at low engine speed operation when the manifold dynamics are neglected, is studied for three possible cases after linearizing the system locally.

(i) Pure Input/Output Phase Lag

Neglecting the manifold air dynamics, equation **(1)** can be written as:

$$\begin{aligned} \dot{\omega}_e &= \frac{1}{I_e}\left[T_{net}(\omega_e, \alpha) - T_L\right] \\ &\triangleq \frac{1}{I_e}\left[u - T_L\right] \end{aligned} \tag{15}$$

and the control law in equation (8) can be written as:

$$u \triangleq T_{net_des} = I_e\left[\dot{\omega}_{e_des} - 2\,\zeta\,\omega_n\,(\omega_e - \omega_{e_des}) - \omega_n^2 \int_0^t (\omega_e - \omega_{e_des})\,dt\right] + T_L \tag{16}$$

Let u have first order lag with a time constant T due to the neglected manifold air dynamics, i.e.:

$$u_1 = -\frac{1}{T}\,u_1 + \frac{1}{T}\,u \tag{17}$$

and

$$\dot{\omega}_e = \frac{1}{I_e}\left[u_1 - T_L\right] \tag{18}$$

Differentiating equation **(17):**

$$\ddot{u}_1 = -\frac{1}{T}\,\dot{u}_1 + \frac{I_e}{T}\left[\ddot{\omega}_{e_des} - 2\,\zeta\,\omega_n\,(\dot{\omega}_e - \dot{\omega}_{e_des}) - \omega_n^2\,(\omega_e - \omega_{e_des})\right] + \frac{\dot{T}_L}{T} \tag{19}$$

Let

$$\dot{\omega}_{e_des} = \ddot{\omega}_{e_des} = \dot{T}_L \triangleq 0 \tag{20}$$

$$u_1 = v_1 \tag{21}$$

$$\dot{u}_1 = v_2 \tag{22}$$

then, equations (18), (19), **(21)** and **(22)** give:

$$\begin{bmatrix} \dot{\omega}_e \\ \dot{v}_1 \\ \dot{v}_2 \end{bmatrix} = \underbrace{\begin{bmatrix} 0 & \frac{1}{I_e} & 0 \\ 0 & 0 & 1 \\ -\frac{I_e\,\omega_n^2}{T} & -\frac{2\,\zeta\,\omega_n}{T} & -\frac{1}{T} \end{bmatrix}}_{\triangleq A} \begin{bmatrix} \omega_e \\ v_1 \\ v_2 \end{bmatrix} + constant \tag{23}$$

The characteristic equation of a matrix $\boldsymbol{A}$ is:

$$\lambda^3 + \frac{1}{T}\lambda^2 + \frac{2\zeta\omega_n}{T}\lambda + \frac{\omega_n^2}{T} = 0 \tag{24}$$

When T, ζ and w, are **0.17, 1.0** and **2.5** as those in figure **4.1,** the solutions **of** equation **(24)** are $\lambda_1 = -1.64, \lambda_{2,3} = -2.12 \pm i4.24,$ and the equivalent cycle time **of** $\lambda_{2,3}$ is **1.48** sec. This is very close to the cycle time in the test$(\approx 1.7\,sec)$. However, the damping of $\lambda_{2,3}$ is too large to have a zero-damping-like mode.

(ii) Pure Input/Output Time Delay

Now assume that the control input u has a pure time delay t_d, i.e.:

$$\begin{aligned} \dot{\omega}_e &= \frac{1}{I_e}[T_{net}(\omega_e, \alpha) - T_L] \\ &\triangleq \frac{1}{I_e}[u_1 - T_L] \end{aligned} \tag{25}$$

$$u = I_e\left[\dot{\omega}_{e_des} - 2\zeta\omega_n(\omega_e - \omega_{e_des}) - \omega_n^2\int_0^t(\omega_e - \omega_{e_des})\,dt\right] + T_L \tag{26}$$

$$u_1(t) = u(t - t_d) \tag{27}$$

Let $\dot{\omega}_{ed} = \ddot{\omega}_{ed} = \dot{T}_L \triangleq 0$ again, then equations **(25)** - **(27)** give:

$$\ddot{\omega}e(t) + 2\zeta\omega_n\dot{\omega}_e(t - t_d) + \omega_n^2\omega_e(t - t_d) = 0 \tag{28}$$

Let

$$\omega_e(t) = e^{i\lambda t} \tag{29}$$

and substituting equation **(29)** into equation (28):

$$-\lambda^2 + i2\zeta\omega_n\lambda e^{-i\lambda t_d} + \omega_n^2 e^{-i\lambda t_d} = 0 \tag{30}$$

If equation **(30)** gives a real valued solution (X, t_d), then the closed-loop system may have a zero damping mode when the time delay is as much as t_d. Since the solution X of equation **(30)** is given as:

$$\mathrm{X} = \sqrt{2\zeta^2 + \sqrt{4\zeta^4 + 1}}\,\omega_n \tag{31}$$

when $\zeta = 1$ and $\omega_n = 2.5,$ X $= 5.1$ and equivalently the cycle time of the mode is **1.23** sec and the required time delay to have that mode is **0.26** sec. This time delay is too much to

exist in this system. Therefore, the system can not have a zero damping mode due to the pure time delay alone.

(iii) Phase Lag Combined with Time Delay

Assume that the control input has both phase lag and time delay, i.e.

$$\dot{\omega}_e = \frac{1}{I_e}\,[u_1 - T_L] \tag{32}$$

$$u = I_e \left[\dot{\omega}_{e_des} - 2\,\zeta\,\omega_n\,(\omega_e - \omega_{e_des}) - \omega_n^2 \int_0^t (\omega_e - \omega_{e_des})\,dt\right] + T_L \tag{33}$$

$$\dot{u}_1 = -\frac{1}{T}u_1(t) + \frac{1}{T}u(t - t_d) \tag{34}$$

Let

$$\dot{\omega}_{e_des} = \ddot{\omega}_{e_des} = \dot{T}_L \triangleq 0 \tag{35}$$

then, equations (32) - (34) give:

$$\dddot{\omega}_e(t) + \frac{1}{T}\ddot{\omega}_e(t) + \frac{2\,\zeta\,\omega_n}{T}\dot{\omega}_e(t - t_d) + \frac{\omega_n^2}{T}\omega_e(t - t_d) = 0 \tag{36}$$

Let equation (36) have a zero damping mode, i.e. $\omega_e(t) = e^{i\lambda t}$, then equation (36) gives:

$$-\frac{1}{T}\lambda^2 + \frac{2\,\zeta\,\omega_n}{T} \times \sin\lambda t_d + \frac{\omega_n^2}{T}\cos\lambda t_d = 0 \tag{37}$$

$$-\lambda^3 + \frac{2\,\zeta\,\omega_n}{T} \times \cos\lambda t_d - \frac{\omega_n^2}{T}\sin\lambda t_d = 0 \tag{38}$$

If equations (37) and (38) have a real valued solution ($\times$, t_d), then the closed-loop system can have a zero damping mode. When T, ζ and ω_n are 0.17, **1.0** and 2.5 as those in figure **4.1,** equations (37) and (38) give a solution $\times = 4.2$, i.e. the cycle time of the zero damping mode is 1.5 *sec*, and the time delay required to get this mode is $t_d = 0.15$ *sec*. The cycle time is very close to that in the test($\approx$ 1.7 *sec*) and the amount of the time delay is reasonable. The intake-to-torque production time delay is around 35 *ms* at 1500 *rpm*[1] and the throttle actuation time delay is around 40 *ms*. In addition, in the first and the second gear states, the torque converter is observed to give 60 - 80 *ms* of time delay. Therefore, the total input/output time delay is 135 - 155 *ms*, and this amount is just enough to generate a low-frequency zero damping mode in the closed-loop system. The amount of time required to generate this mode by the pure time delay alone is 260 *ms*, so 110 *ms* safety margin is obtained by considering the manifold air dynamics in the control.

5 Ultrasonic ranging system

5.1 Introduction

This section describes a Polaroid-based ultrasonic ranging system. This system uses 50 kHz ultrasonic sound and the operating range is approximately 0.15 - 10 meters. The typical absolute accuracy is ± 1 % of the reading over the entire range. In operation, a pulse is transmitted toward a target and the resulting echo is detected. The elapsed time between initial transmission and echo detection can then be converted to distance with respect to the speed of sound.

The speed of sound at 20°C is 343.2 m/s. It varies only slightly with humidity(max 0.35 % at 20°C) and is virtually independent of pressure and, thus, of height above sea level.

5.2 System Description

The system should respond only to echoes from objects which fall within a given solid angle around the transmit axis. Any echo signal from an object far off the axis is undesirable. Transducer diameter and transmit frequencies were chosen so that an object at a distance of 25 cm at an angle of **20** degrees gives an echo about **20** dB weaker than the same object placed on axis at the same distance. If the object is moved from 25 cm to a distance of 5 rn on axis, the echo will fall off by about 60 dB.

If a constant amplification were used the operating range would be severely limited. The situation is even worse since different objects at different temperatures and humidities will vary in echo strength by as much as 20 - 30 dB. Therefore, it is desirable to vary the amplification with distance: low amplification for near distance echoes, high amplification for far distance echoes. Since the roundtrip time for the signal is proportional to the distance, the amplification should be increased as a function of time. The gain should not produce a constant signal level of a given object at different distances. It is assumed that nearer objects tend to be smaller and therefore relatively more gain is desirable(figure 5.1). Large amplified signals improve the accuracy of the distance determination, but make the system more sensitive to **small** particles between the transducer and the target[3][4].

5.3 Field Test

The ultrasonic ranging system was tested at the California Highway Patrol(CHP) Academy test track at Sacramento. It is a windy area and the track is dusty. The test was performed using two Lincoln TownCars with one following the other. Figure 5.2 shows

that the system works well at low vehicle speed and within its operating range. However, figure **5.3** shows that, even when the distance is within the operating range, it produces only noise at the higher vehicle speed. There are three possible sources of the noise: wind noise, tire noise and dust/particles. The effect of the wind noise can be checked easily by driving the vehicle at high speed without any target vehicle, and it was found not to be a source of the noise. Second, it was tested using two vehicles at high speed but in a relatively clean section of the track, and there was not much noise. So, it is concluded that the noise comes from the cloud of dust kicked up by the lead vehicle at high speeds. The noise was also found to disappear if the vehicles drive very fast at too short a distance for the kicked up dust to appear between them.

As described **in** section 5.2, the system gain is varied such that it is very sensitive to any particles which are very close to the transmitter. So, this system may not be appropriate for use in a dusty environment.

6 Multi-Vehicle Test

In section **4,** several longitudinal control laws were compared by field test, and the control law based on a full engine model including the manifold dynamics showed the best tracking performance.

In this section, multi-vehicle closed-loop control is tested using the best control law during low speed cruising. The control law obtains distance and closing rate data from the ultrasonic ranging unit and the lead vehicle speed transmitted by radio.

Figure 6.1 shows the test result of the multi-vehicle tracking control. The ranging unit works well most of the time since the vehicle speeds are very low, and the distance between the two vehicles converges to the preset value exponentially as desired. The throttle does not chatter much, so the ride quality, i.e. the vehicle acceleration history, is quite smooth.

7 Conclusions

Several longitudinal vehicle control laws and an ultrasonic ranging system were evaluated during field tests. The test results show that the Polaroid-based ranging system is very sensitive to small particles at close distance and may not be appropriate for the harsh conditions of vehicle operation on the highway.

Input/output phase lag combined with time delay increases the order of the closed-loop system, and an undesirable zero damping mode can be generated. This can be prevented by

adopting a full engine model for the control. The full model gives a margin of safety to the input/output time delay by about 110 ms which may vary depending upon the operating conditions of the engine.

Acknowledgements

The author wishes to thank Bob Battersby of the Caltrans New Technology staff for his assistance in arranging the use of test facilities at the CHP Academy, and Pete Devlin of California PATH for his assistance throughout the test program.

References

[1] D. Cho and J.K. Hedrick, "Automotive Powertrain Modeling for Control", ASME Transactions on Dynamic System, Measurements and Control, Vol. **111,** December, **1989.**

[2] S.-B. Choi and J.K. Hedrick, "Design of a Robust Controller for Automotive Engines: Theory and Experiment", Ph.D. Thesis, Vehicle Dynamics and Control Lab., U.C. Berkeley, August, **1993.**

[3] Polaroid Corporation, "Polaroid Ultrasonic Ranging System Handbook, Application Notes/Technical Paper".

[4] Polaroid Corporation, "Ultrasonic Ranging System", Telephone **1-800-225-1618.**

[5] J.J.E. Slotine and W. Li, "Applied Nonlinear Control", Prentice Hall, **1991.**

[6] D. Swaroop, J.K. Hedrick, C.C. Chen and P. Ioannou, "A Comparison of Spacing and Headway Control Laws for Automatically Controlled Vehicles", PATH Report, **1993.**

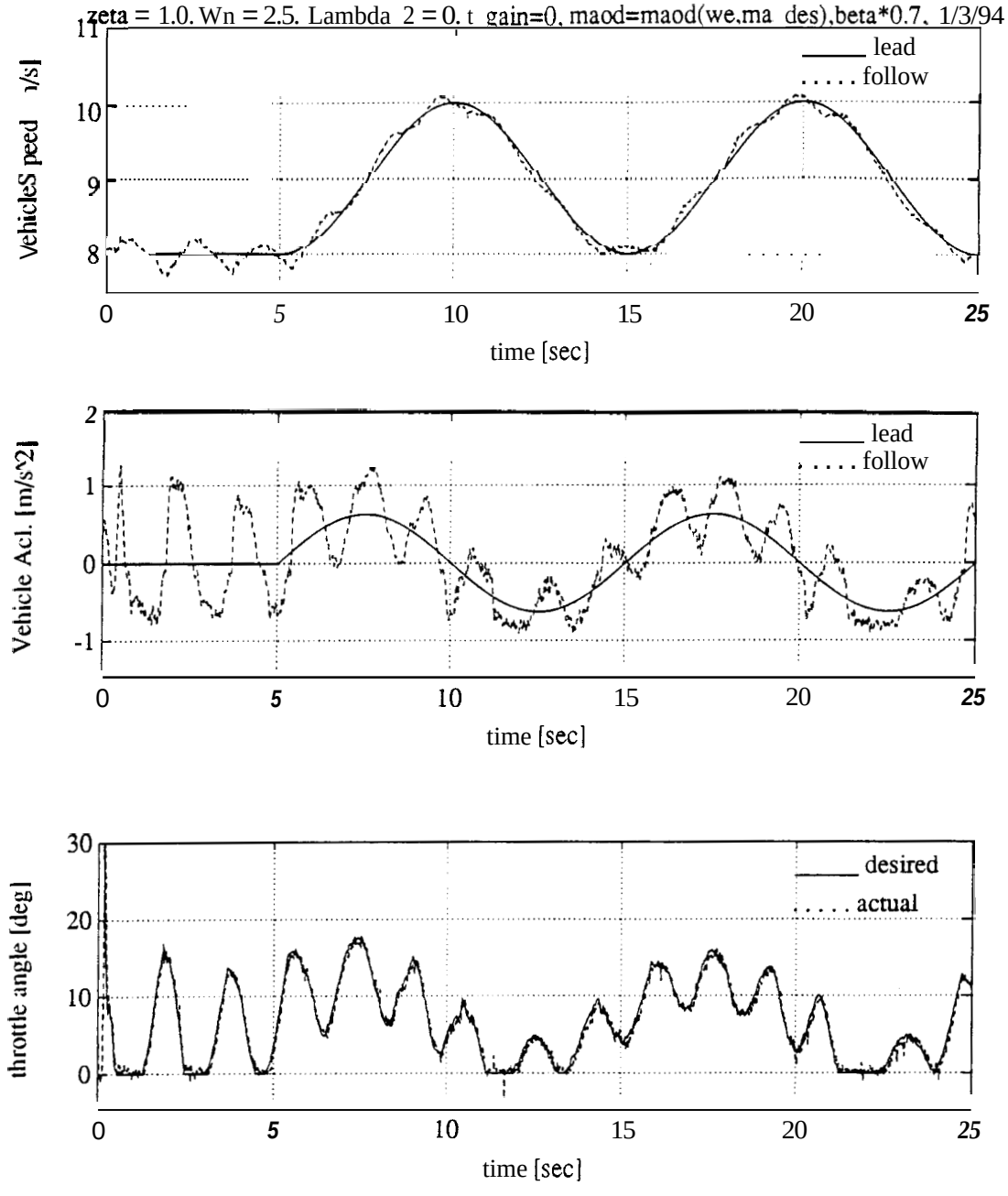


Figure 4.1: Single vehicle tracking control; simple model, no torque converter

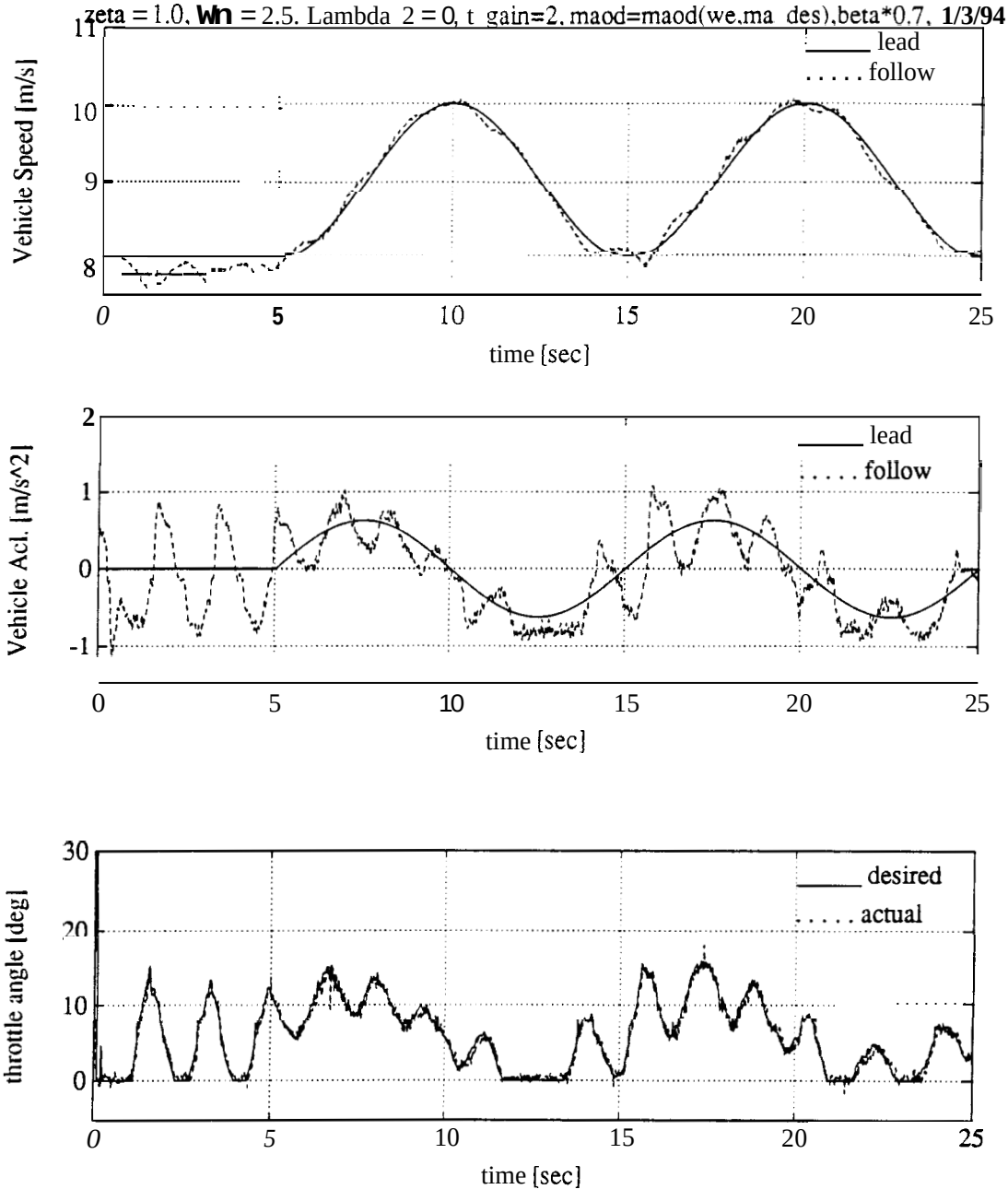


Figure 4.2: Single vehicle tracking control; simple model with torque converter

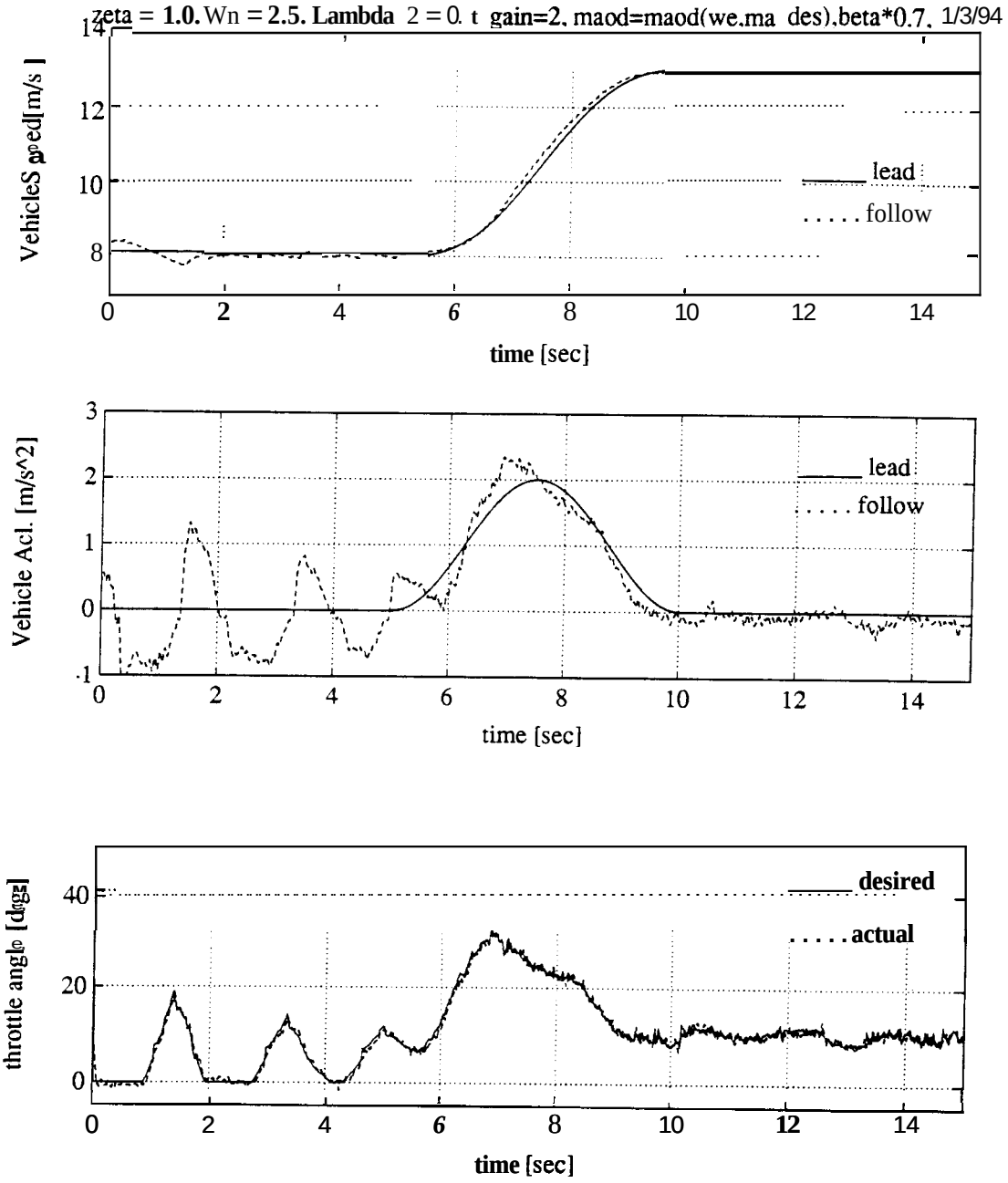


Figure 4.3: Single vehicle tracking control; simple model with torque converter

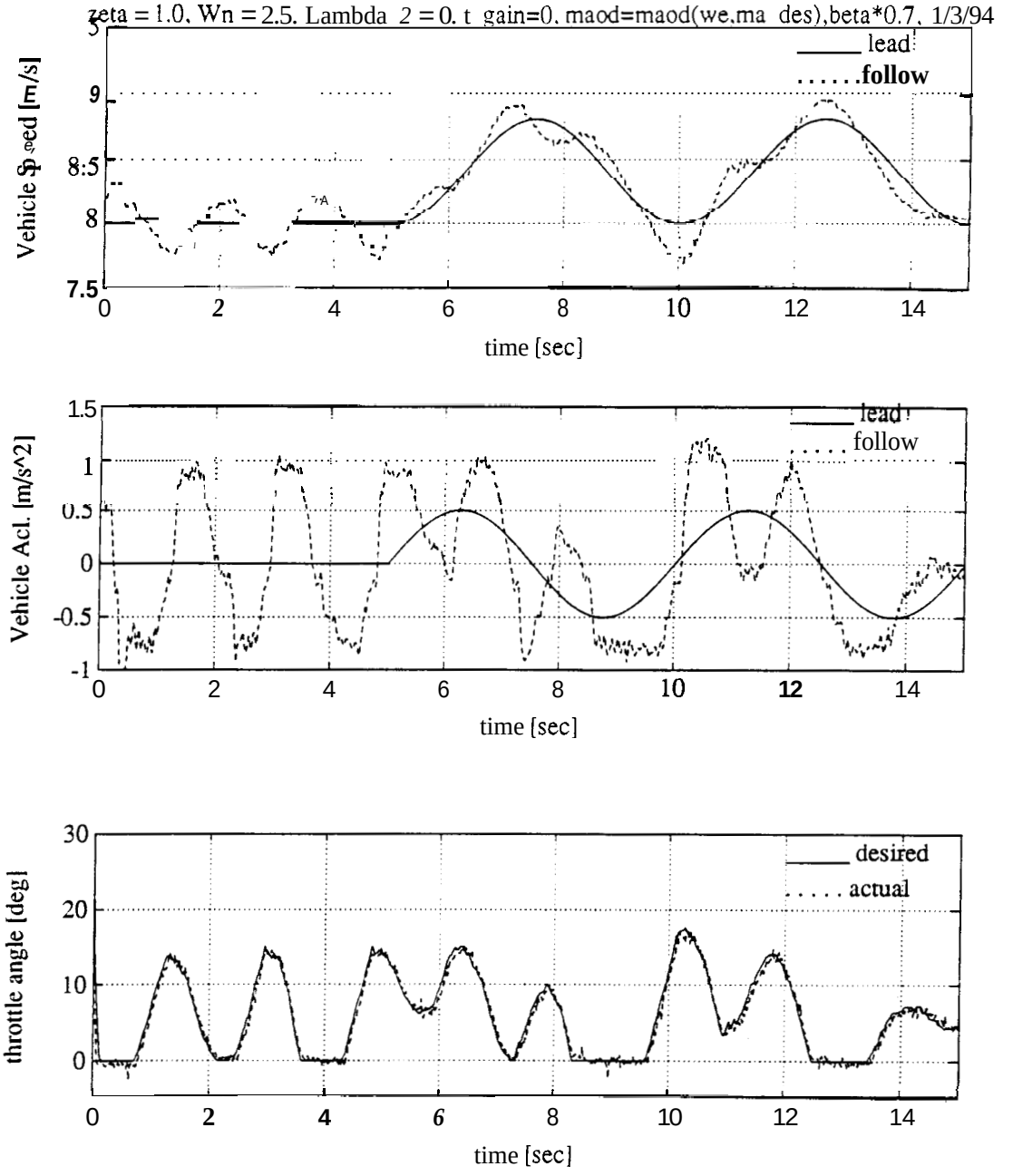


Figure **4.4:** Single vehicle tracking control; simple model with torque converter

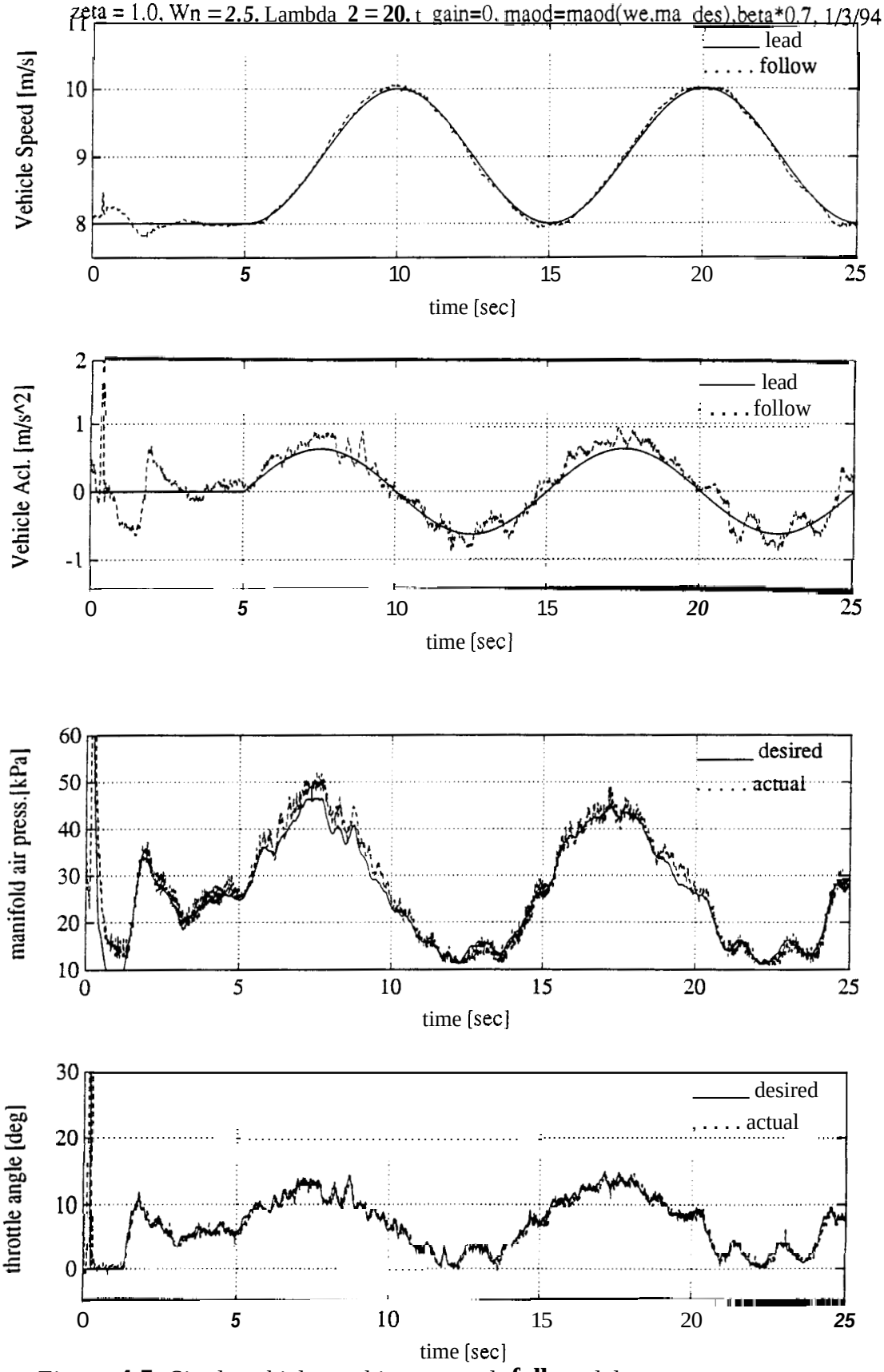


Figure **4.5:** Single vehicle tracking control; **full** model, no torque converter

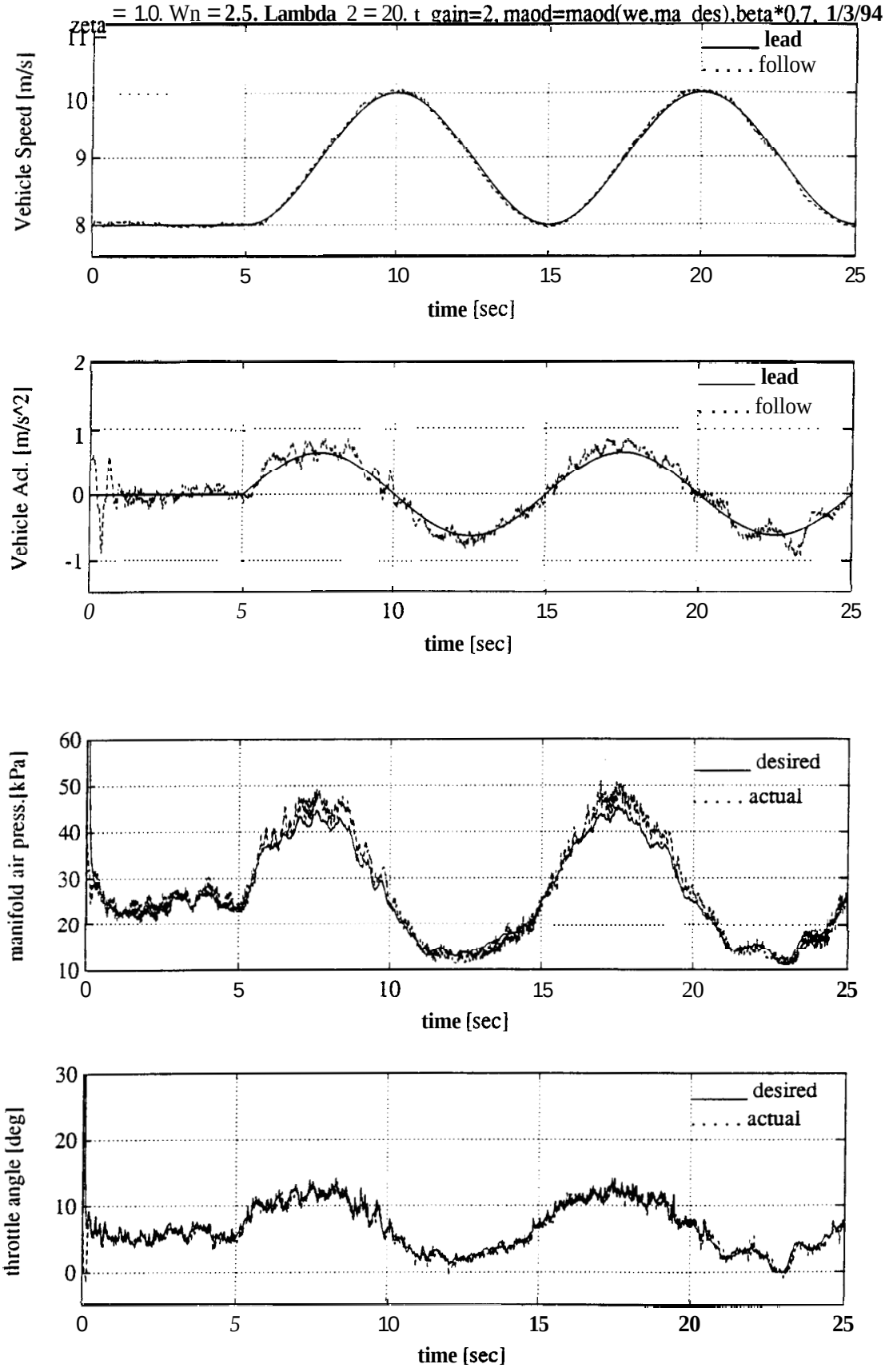


Figure 4.6: Single vehicle tracking control; full model with torque converter

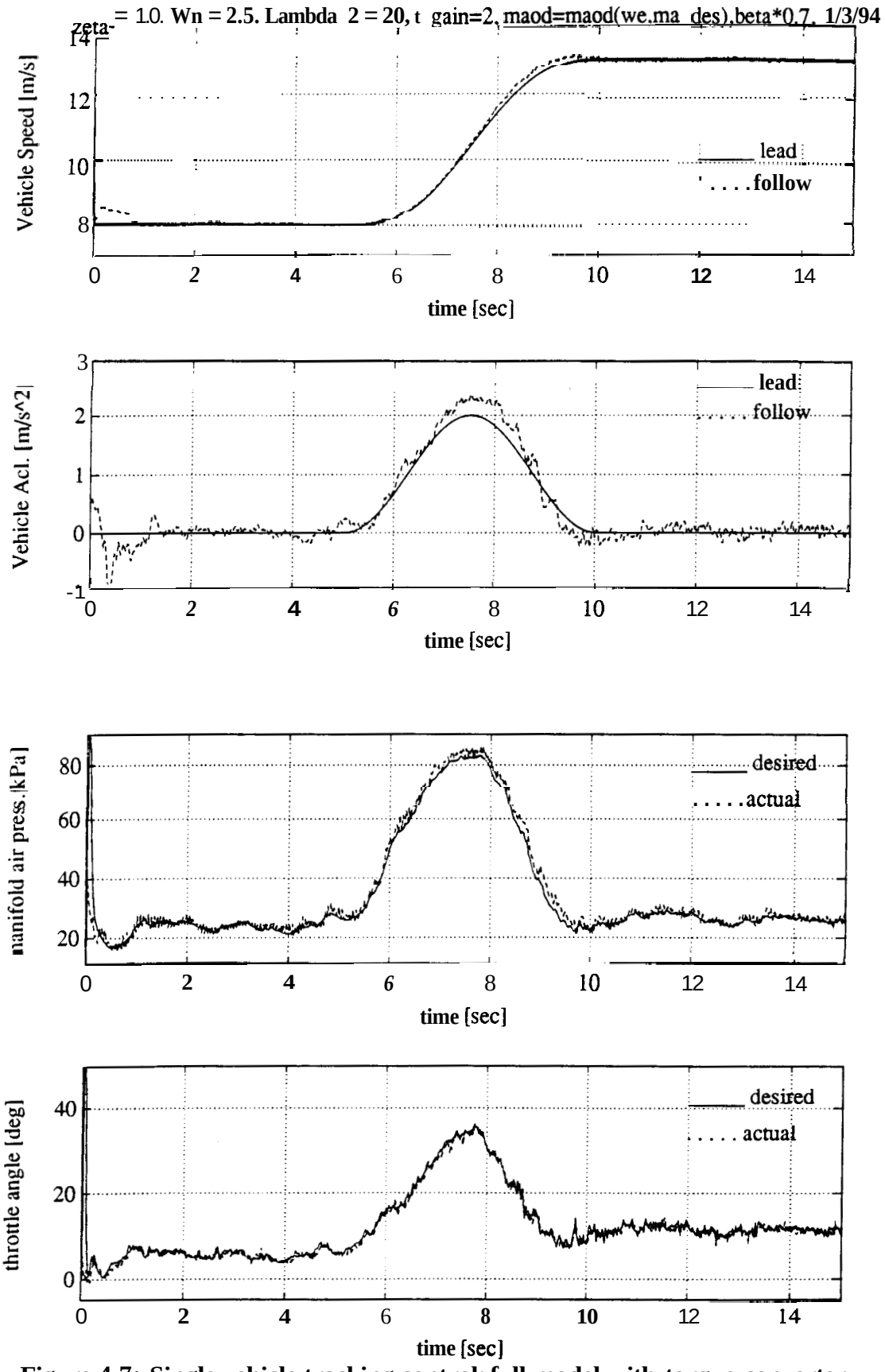


Figure 4.7: Single vehicle tracking control; full model with torque converter

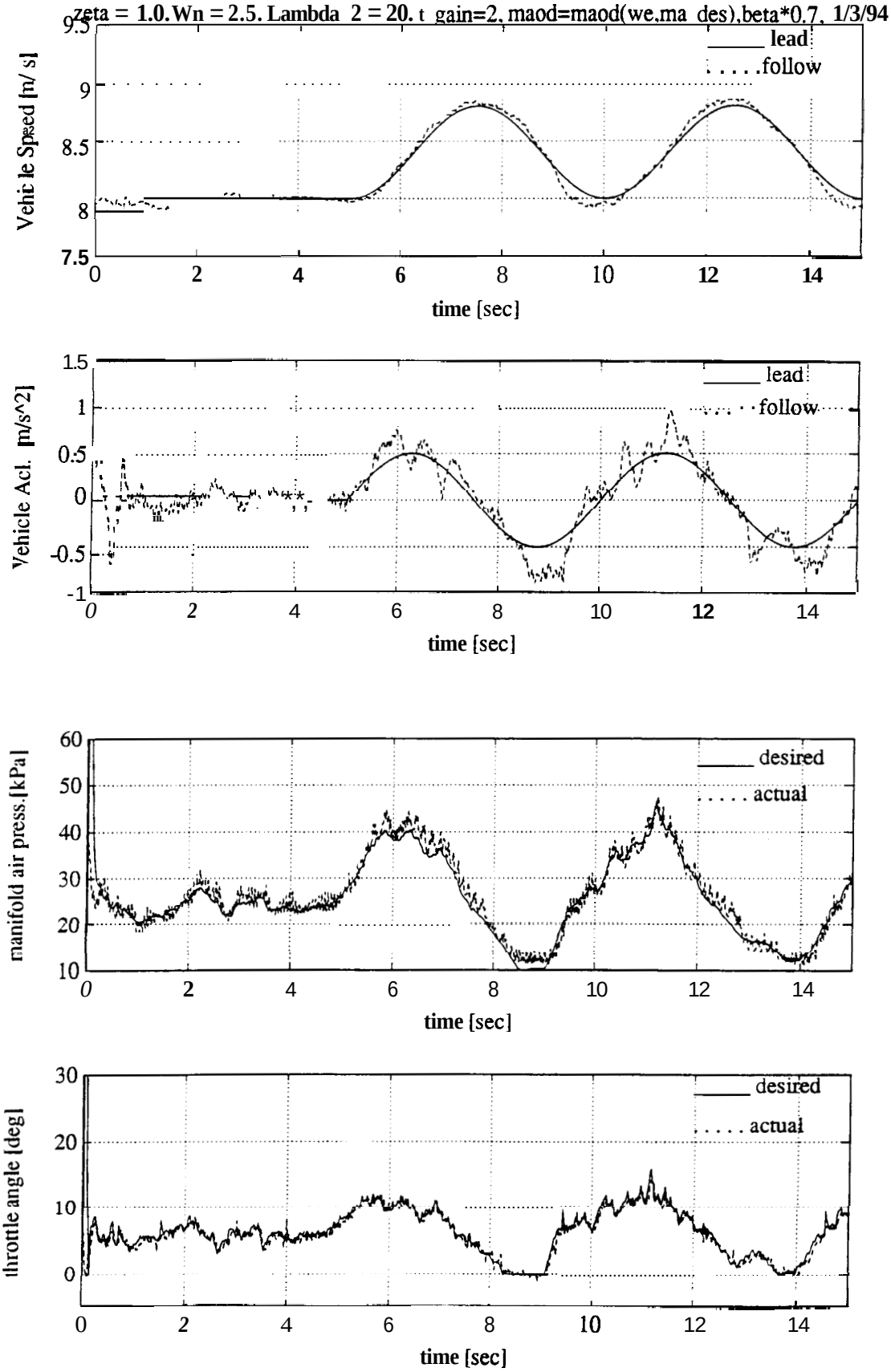


Figure 4.8: Single vehicle tracking control; full model with torque converter

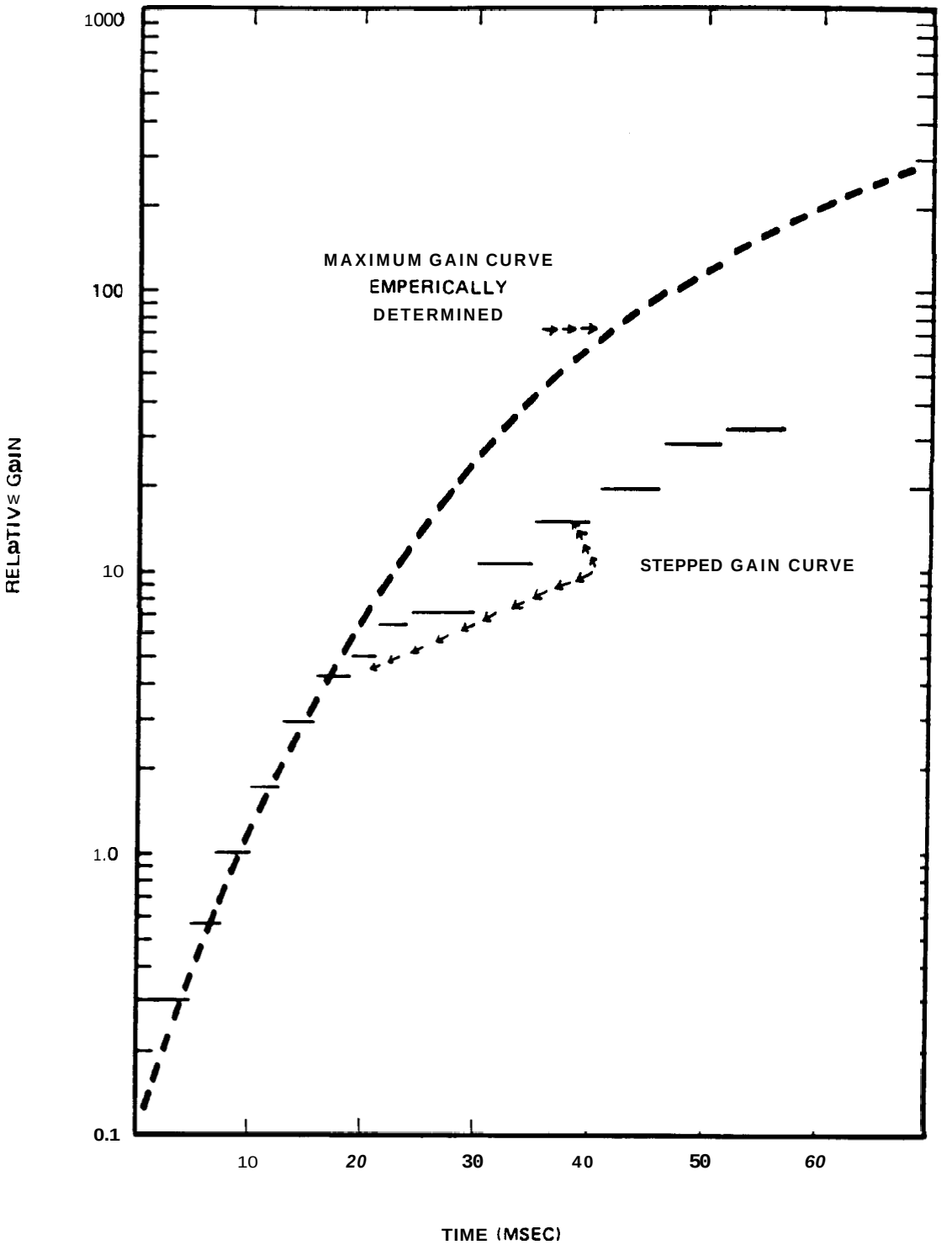


Figure 5.1: Polaroid ranging system; gain scheduling curve

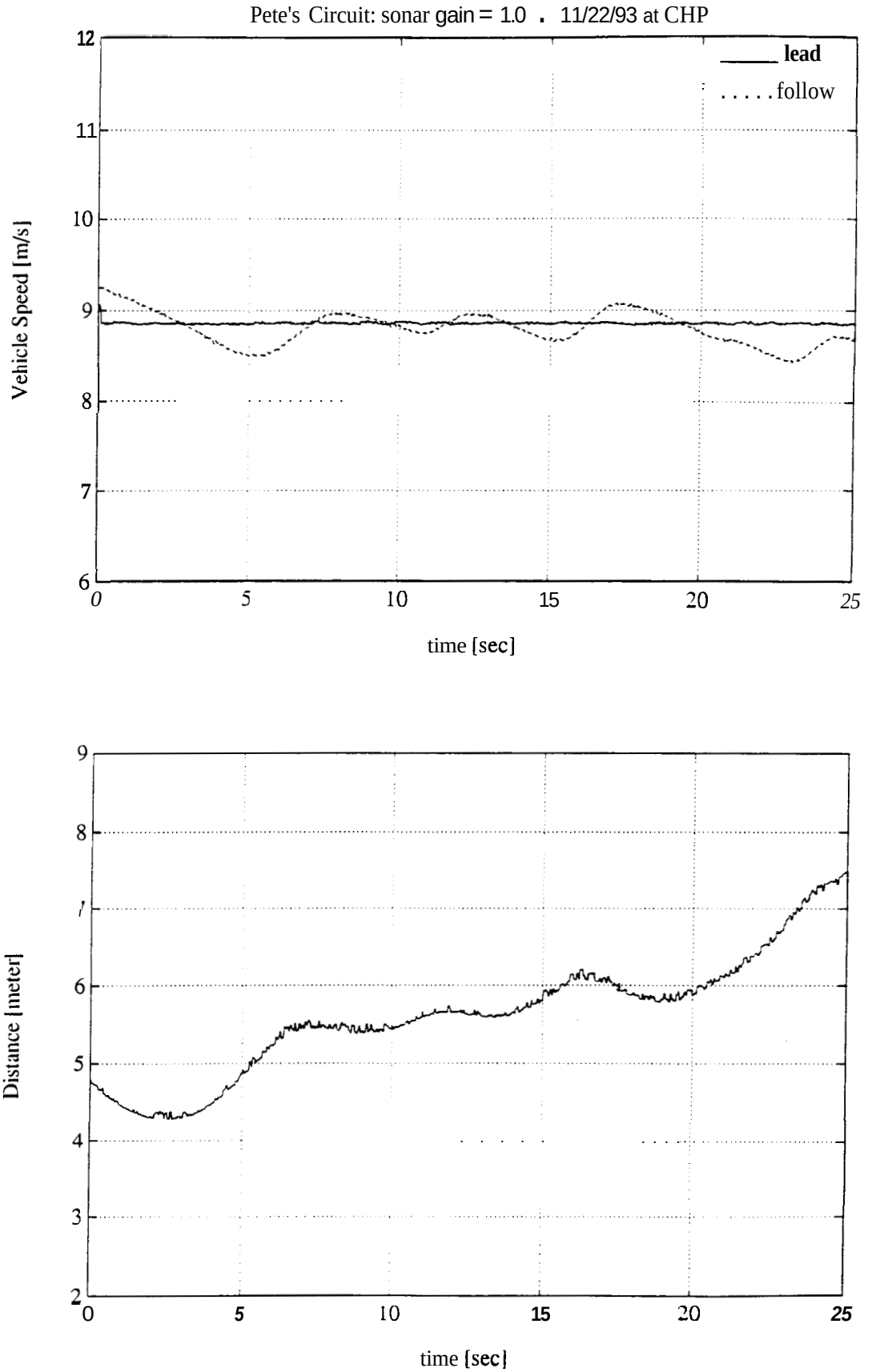
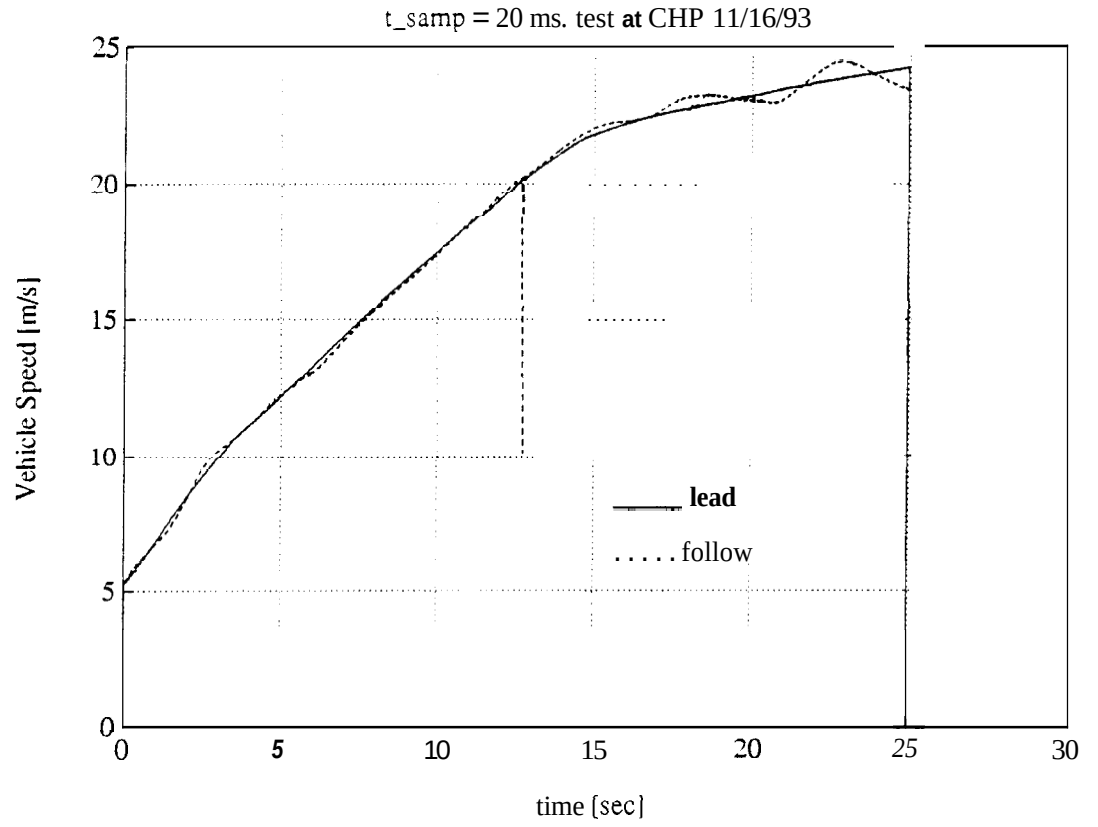


Figure 5.2: Polaroid ranging system; low speed test



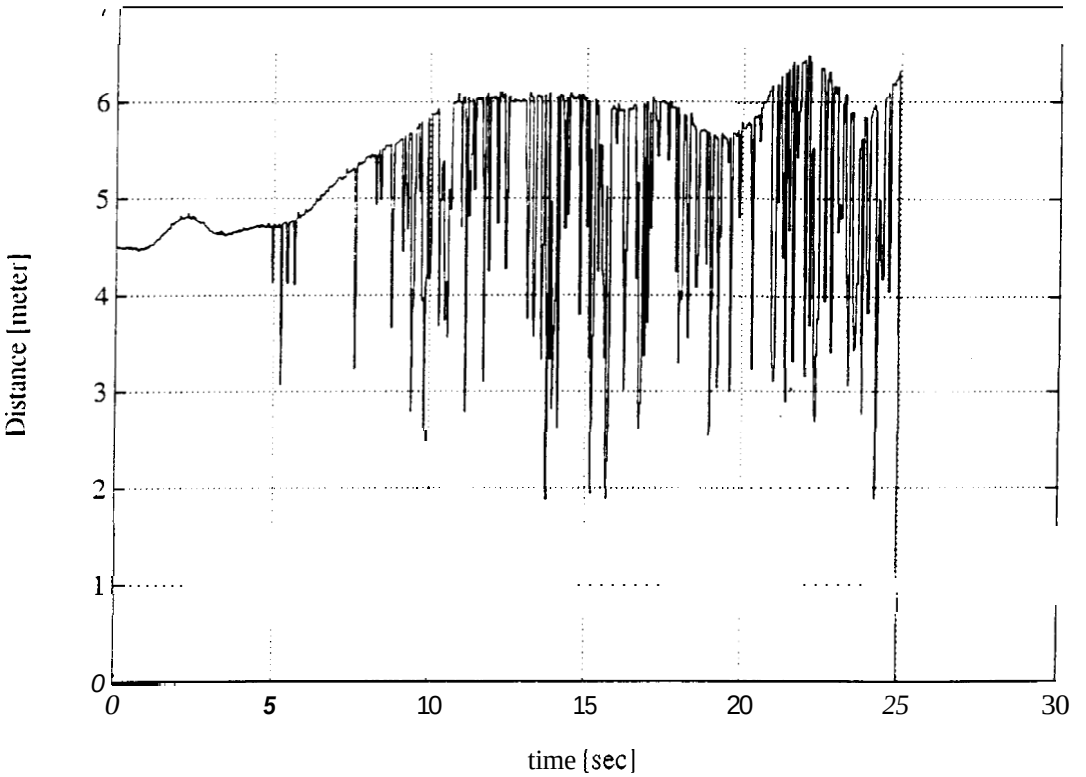


Figure **5.3:** Polaroid ranging system; high speed test

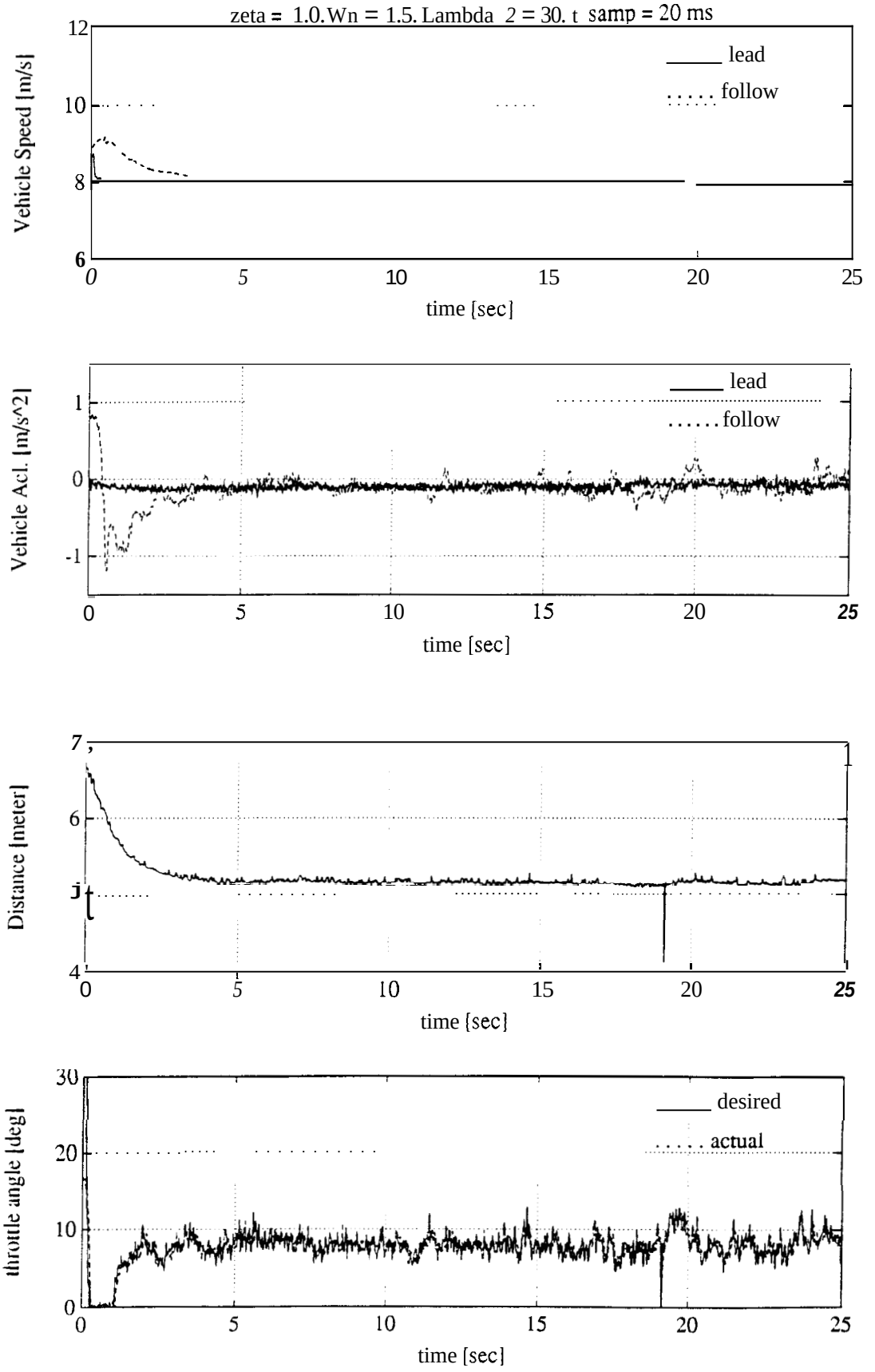


Figure 6.1: two vehicle tracking control; full model, no torque converter